Volume 10 | Number 44 | 28 November 2019 | Pages 5941–6064

Polymer Chemistry

rsc.li/polymers

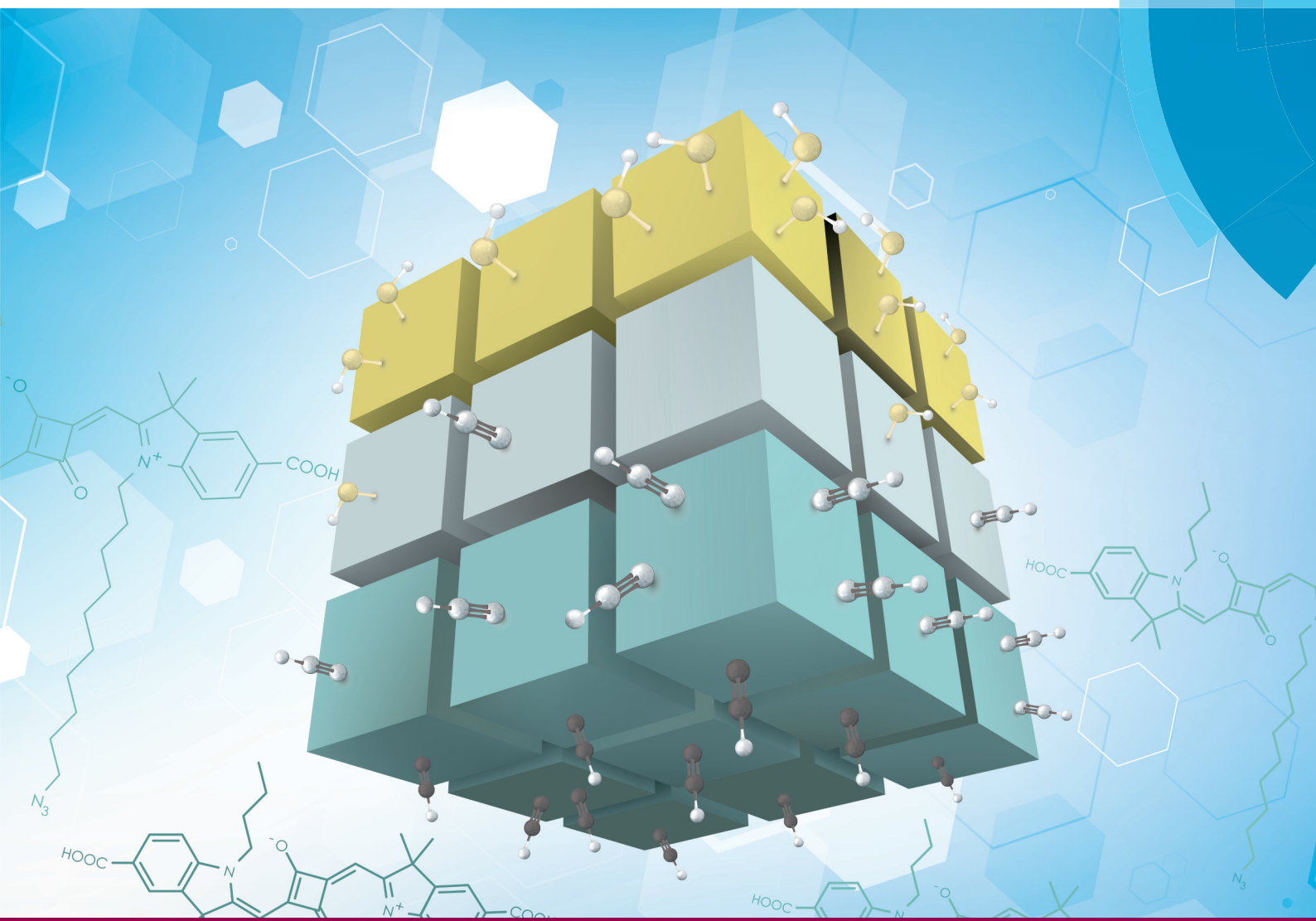

Themed issue: Includes a collection on chemical advances in additive manufacturing

ISSN 1759-9962

ROYAL SOCIETY OF CHEMISTRY | Celebrating IYPT 2019

PAPER
Annalisa Chiappone *et al.*
Thiol–yne chemistry for 3D printing: exploiting an off-stoichiometric route for selective functionalization of 3D objects

Polymer Chemistry

PAPER

View Article Online
View Journal | View Issue

Cite this: *Polym. Chem.*, 2019, **10**, 5950

Thiol–yne chemistry for 3D printing: exploiting an off-stoichiometric route for selective functionalization of 3D objects†

Ignazio Roppolo,[a] Francesca Frascella,[a] Matteo Gastaldi,[b] Micaela Castellino,[a] Betty Ciubini,[a] Claudia Barolo,[b] Luciano Scaltrito,[a] Carmelo Nicosia,[c] Marco Zanetti[b,d] and Annalisa Chiappone*[a]

An alkyne monomer bis(propargyl) fumarate is synthesized and used to produce DLP-3D printable formulations with a thiol exploiting photoinduced thiol–yne reaction. By preparing mixtures containing different relative ratios of two monomers, it is possible to obtain polymers exposing different unreacted functional groups on their surface. The reactivity of the formulations toward visible light irradiation is studied by ATR analysis and photorheology tests, the printability with DLP equipment is demonstrated and the thermo-mechanical properties of the obtained polymers are investigated by DMA. Changing the printing formulation during the printing process, objects exposing either triple bonds or thiol groups or a mix of them can be obtained, and the presence of unreacted groups is confirmed by XPS analysis; this property can be exploited to selectively functionalize the built parts in a dedicated post process. As a proof of concept, a simple hybrid structure is treated with an azide-terminated squaraine dye, to exploit a 'click' reaction with the alkyne groups available. The fluorescence of the functionalized structure is observed with a spinning disk confocal microscope. Such a strategy can allow producing 3D objects with a controllable structure just by varying the relative ratio of the co-monomers in the formulations during the printing process.

Received 30th June 2019,
Accepted 6th September 2019

DOI: 10.1039/c9py00962k

rsc.li/polymers

Introduction

3D printing is a production technique that allows fabricating objects starting from CAD files by adding materials in a layer by layer fashion.[1] The techniques comprised under this umbrella term enable the fabrication of extremely complex shapes without material waste and without using moulds.[2,3] This makes 3D printing a step-forward and fascinating alternative to the most common subtractive manufacturing procedures.[4–6]

In the last decades several types of 3D printing machines have been developed and optimized; they differ from each other in terms of the technology that they exploit and the typology of printable materials.[1] Just considering the polymeric materials, many different classes of 3D printers can be listed; some examples are as follows: FFF (Fused Filament Fabrication), the most diffused technique that uses thermoplastic filaments, heated and deposited layer by layer;[7] SLS (Selective Laser Sintering), which sinters thermoplastic powders with a laser to obtain 3D objects;[8] SL (Stereo Lithography) and its close relative DLP (Digital Light Processing), which print thermoset polymers starting from liquid photocurable formulations. Those mixtures are usually based on (meth)acrylic monomers.[9,10] Each technique has its advantages and drawbacks and the choice of a particular one can be related to the specific application.[11] Nowadays, all the 3D printing techniques are largely investigated at the academic level and in some cases additive manufacturing products are proposed at the commercial level.[1,12]

To further expand the possibilities given by 3D printing, functional 3D shaped objects can be fabricated.[13,14] In this work, we developed new functional materials for photopolymerization based processes, in particular DLP.[15]

Intrinsically functional 3D printable materials for DLP or SL have been previously proposed;[15] in this case, several routes can be followed, such as the addition of nanofillers,[13,16–18] the use of stimuli responsive,[19] conductive[20] or shape memory polymers[21] and smart dyes[22,23] and many others.[15,24]

[a]*Department of Applied Science and Technology DISAT, Politecnico di Torino, Corso Duca degli Abruzzi, 24, Torino, 10129, Italy.*
E-mail: Annalisa.chiappone@polito.it
[b]*Department of Chemistry and NIS Centre, University of Turin, Via P. Giuria 7, Torino, 10125, Italy*
[c]*Department of Electronics and Telecommunications DET, Politecnico di Torino, Corso Duca degli Abruzzi, 24, Torino, 10129, Italy*
[d]*ICxT Centre, University of Turin, Lungo Dora Siena 100, Torino, 10153, Italy*

†Electronic supplementary information (ESI) available: NMR spectra, photorheology plot, ATR Spectra and DSC with details on the formulations. See DOI: 10.1039/c9py00962k

Another suitable approach consists of exploiting a post functionalization step on the 3D printed objects; this results in particular interest for the introduction of biofunctional molecules, as largely demonstrated for different polymeric surfaces.[25] To do this, chemically reactive moieties can be directly introduced in the DLP printable liquid formulations, aiming to exploit their available groups for further functionalization steps.

Stassi *et al.*[26] printed micrometric cantilevers by DLP starting from an acrylate-based formulation in which acrylic acid was added. Its carboxylic groups were exploited to functionalize the cantilever surface. Alternatively, Wang *et al.*[27] incorporated a vinyl-terminated initiator into a curable resin to obtain functional structural materials that enabled a post-printing surface-initiated ATRP modification.

The addition of chemical moieties that can easily react in a dedicated functionalization step could enable a wide range of reactions for the modification of 3D printed objects.[28,29] In this work, we propose the use of 3D printable thiol–yne monomers to obtain objects that can be easily post functionalized.[30,31]

Thiol–yne polymerization has been studied for many decades,[32–35] but in the last years it attracted increasing interest in the field of photopolymerization[36] as well as thiol–ene reactions,[37] since it presents many advantages over the more common traditional radical chain-growth polymerizations.[38]

Alkyne monomers can be easily synthesized in different structural formats. In the thiol–yne reaction each alkyne functional group can react consecutively with two thiol functional groups; this leads to the formation of highly crosslinked networks presenting high toughness and good thermo-mechanical properties, beyond their known biocompatibility.[39] These intriguing properties make thiol–yne photopolymerization an interesting route for the production of films with good mechanical properties.[36] But, moving a step ahead, this kind of chemistry can also be applied to DLP and SL 3D printing, allowing the production of 3D materials presenting the aforementioned characteristics.[40]

To allow an easy post-functionalization of these 3D printable materials, we propose the development of off-stoichiometric formulations: in this way, after the printing process, an excess of SH (thiol) or YNE (alkyne) functionalities that are not involved in the cross-linked network become available for a variety of post-functionalization processes. As Carlborg *et al.*[41] introduced the idea of using OSTE (off-stoichiometric thiol–ene) formulations mainly for developing functionalized microfluidic channels[42] and Hoffmann *et al.* applied them in 3D sterelitograpy,[43] in this paper we prepare OSTY (off-stoichiometric thiol–yne) formulations. After the synthesis of the alkyne monomer (bis(propargyl) fumarate), we demonstrate its printability and the possibility of post functionalizing the 3D printed parts. Such a strategy can allow the production of 3D objects with controllable networks, just by varying the relative ratio of the co-monomers in the formulations during the printing process.

Experimental

Materials

All chemicals were purchased from Sigma-Aldrich, Fluka, Merck Riedel de Haen and Alfa Aesar, unless otherwise noted, and were used as received. The synthesis of squaraine was carried out with a microwave BIOTAGE® Isolera Iniziator + 2.5. All flash purifications were performed with a BIOTAGE® Isolera™ using a Biotage® SNAP Ultra silica gel column. TLC was performed on silica gel 60 F254 plates.

Trimethylolpropane tris(3-mercaptopropionate) (Sigma-Aldrich) was used as a thiol comonomer, and phenylbis(2,4,6-trimethylbenzoyl) phosphine oxide (BAPO, Sigma-Aldrich) was used as a photoinitiator.

Synthesis of bis(propargyl) fumarate – an alkyne monomer (Scheme 1)

The reaction, requiring anhydrous conditions, was conducted in flame-dried glassware under an argon atmosphere. As reported in Scheme 1, propargyl alcohol(II) (7.55 mL, 131 mmol) was dissolved in anhydrous dichloromethane (50 mL) in a three-neck round-bottom flask equipped with a stir bar and a dropping funnel. Triethylamine (21.88 ml, 157.2 mmol) was added, and the mixture was cooled to 0 °C. A solution of fumaryl chloride(I) (5.65 mL, 52.4 mmol) in anhydrous CH_2CI_2 (30 mL) was added dropwise over 45 minutes. The reaction mixture was allowed to reach room temperature, stirred for 24 hours, then washed sequentially with saturated ammonium chloride (3 × 250 mL), saturated sodium bicarbonate (2 × 240 mL) and brine (1 × 80 mL) before being dried, and filtered and the solvent was evaporated. This provided a crude material as a dark brown solid which was purified by flash column chromatography (isocratic elution with 100% diethyl ether) to obtain the product in 81 percent yield as a brown white solid.[44] R_f 0.87 (100% diethyl ether); ^{1}H NMR (600 MHz, chloroform-d): δ 6.93 (s, 2H), 4.80 (d, J = 2.5 Hz, 4H), 2.52 (t, J = 2.5 Hz, 2H), ^{13}C NMR (151 MHz, chloroform-d): δ 163.99, 133.69, 75.89, 75.39, 52.64.

Synthesis of 4-((1-(10-azidodecyl)-5-carboxy-3,3-dimethyl-3*H*-indol-1-ium-2-yl)methylene)-2-(((*E*)-1-butyl-5-carboxy-3,3-dimethylindolin-2-ylidene)methyl)-3-oxocyclobut-1-en-1-olate – azide terminated squaraine dye (5) (Scheme 2)

Synthesis of 1-butyl-5-carboxy-2,3,3-trimethyl-3*H*-indol-1-ium iodide (1). The procedure followed is the same as reported by N. Barbero *et al.*[45] 2,3,3-Trimethyl-3*H*-indole-5-carboxylic acid (2.50 g, 12.3 mmol), 1-iodobutane (5.6 ml, 49.2 mmol) and 9 ml CH_3CN.

Yield: 86% (4.10 g, 10.6 mmol).

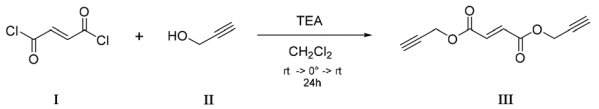

Scheme 1 Synthesis of bis(propargyl) fumarate. Experimental conditions: R: Et_3N, S: CH_2Cl_2, 45 min, 0 °C; 0 °C → rt; 24 h, rt.

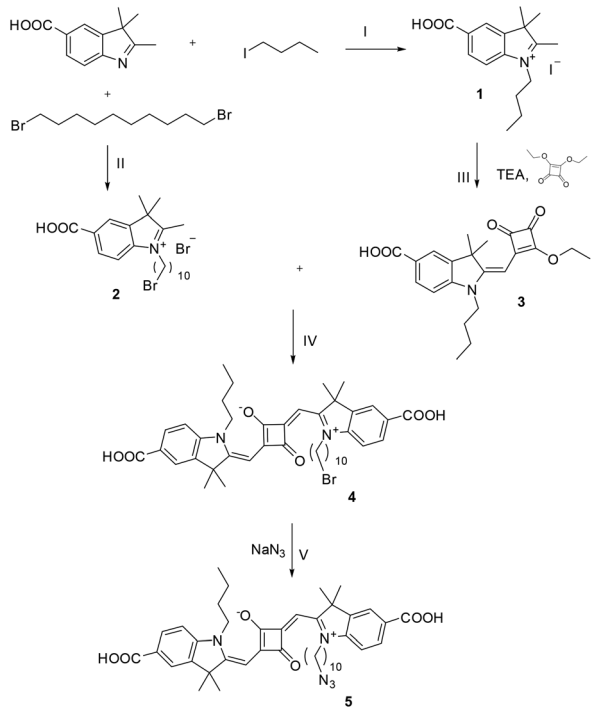

Scheme 2 General procedure for the synthesis of squaraine. (I) Anhydrous CH_3CN, MW: T = 155 °C, t = 20 min. (II) Anhydrous CH_3CN, MW: T = 165 °C, t = 60 min. (III) EtOH, MW: T = 90 °C, t = 13 min. (IV) BuOH/toluene, MW: T = 160 °C, t = 60 min. (V) DMF, MW: T = 100 °C, t = 20 min.

^{1}H NMR (200 MHz, DMSO-d6): δ = 8.39 (s, 1H), 8.14 (m, 2H), 4.49 (m, 2H), 2.92 (s, 3H), 1.83 (m, 2H), 1.58 (s, 6H), 1.46–1.40 (m, 2H), 0.93 (t, 3H). Characterization is in agreement with the literature.

Synthesis of 1-(10-bromodecyl)-5-carboxy-2,3,3-trimethyl-3*H*-indol-1-ium bromide (2). 2,3,3-Trimethyl-3*H*-indole-5-carboxylic acid (0.500 g, 2.46 mmol) was put in a microwave vial with a magnetic stirrer. The vial was sealed and 1,10-dibromodecane (3.69 g, 2.76 ml, 12.3 mmol) was added using a syringe along with 8 ml of anhydrous acetonitrile. Ar was fluxed for 15 minutes, and then the reaction was carried out in microwave (T = 165 °C, 60 minutes). The solvent was removed under vacuum and the product was recovered with ethyl ether, filtered and washed five times with ethyl ether.

Yield 73% (0.903 g, 1.80 mmol).

^{1}H-NMR (200 MHz, DMSO-d6) δ (ppm) = 8.40 (s, 1H), 8.13 (m, 2H), 4.48 (t, 2H), 3.51 (t, 2H), 2.89 (s, 3H), 1.77 (t, 2H), 1.58 (s, 6H), 1.26 (m, 14H).

Synthesis of 1-butyl-2-((2-ethoxy-3,4-dioxocyclobut-1-en-1-yl) methylene)-3,3-dimethylindoline-5-carboxylic acid (3). 1-Butyl-5-carboxy-2,3,3-trimethyl-3*H*-indol-1-ium (0.100 g, 0.258 mmol) was put in a microwave vial, equipped with a magnetic stirrer. Then ethanol (3 ml), 3,4-diethoxycyclobut-3-ene-1,2-dione (0.088 g, 0.08 ml, 0.52 mmol) and triethylamine (0.078 g, 0.11 ml, 0.78 mmol) were added. The reaction was carried out in microwave (T = 90 °C, 13 minutes). The crude material was evaporated, recovered with ethyl ether and filtrated under vacuum: the obtained solid was washed with ethyl ether (3 × 15 ml). The product was purified by flash column chromatography (EtOAc : petroleum ether 3 : 7).

Yield: 49% (48.5 mg, 0.126 mmol).

R_f: 0.28 (EtOAc : petroleum ether 3 : 7).

^{1}H NMR (200 MHz, DMSO-d6) δ (ppm) = 7.93 (s, 1H), 7.865 (d, 1H, J = 6.0 Hz), 7.24 (d, 1H, J = 8.0 Hz), 5.44 (s, 1H), 4.82 (m, 2H), 3.93 (t, 2H, J = 8.0 Hz), 1.56 (s, 6H), 1.41 (m, 4H), 0.88 (t, 3H, J = 8.0 Hz).

^{13}C NMR (50 MHz, DMSO-d6) δ (ppm) = 192.88, 188.93, 187.24, 172.51, 167.10, 146.40, 140.28, 130.38, 124.42, 122.76, 108.67, 82.192, 70.04, 46.962, 42.12, 28.05, 26.47, 19.39, 15.56, 13.54.

ESI-MS: 382.44 (M-1).

Synthesis of 4-((1-(10-bromodecyl)-5-carboxy-3,3-dimethyl-3*H*-indol-1-ium-2-yl)methylene)-2-((-1-butyl-5-carboxy-3,3-dimethylindolin-2-ylidene)methyl)-3-oxocyclobut-1-en-1-olate (4). 1-(10-Bromodecyl)-5-carboxy-2,3,3-trimethyl-3*H*-indol-1-ium bromide (0.145 g, 0.289 mmol) and 1-butyl-2-((2-ethoxy-3,4-dioxocyclobut-1-en-1-yl)methylene)-3,3-dimethylindoline-5-carboxylic acid (0.111 g, 0.289 mmol) were put in a vial and dissolved in butanol (1 ml) and toluene (1 ml). The vial was sealed and the reaction was carried out in microwave (T = 160 °C, 1 hour). A green-blue liquid was recovered with ethyl ether and the solvent was evaporated. The product was re-crystallised from butanol and the obtained solid was filtered under vacuum, washed with ethyl ether and dried in a vacuum stove (40 °C, 2 hours).

Yield: 24% (0.052 g, 0.069 mmol).

R_f: 0.71 (MeOH : $CHCl_3$ 1 : 9).

^{1}H NMR (200 MHz, DMSO-d6) δ (ppm) = 8.03 (s, 2H), 7.96 (d, 2H, J = 8.0 Hz), 7.43 (d, 2H, J = 8.0 Hz), 5.90 (s, 2H), 4.12 (t, 4H, J = 6.0 Hz), 3.47 (t, 2H, J = 7.0 Hz), 1.70 (m, 12H), 1.23 (m, 20H), 0.94 (t, 3H, J = 8.0 Hz).

^{13}C NMR (50 MHz, DMSO-d6) δ (ppm) = 180.92, 170.18, 167.46, 146.35, 141.96, 130.69, 126.29, 123.66, 119.66, 110.67, 88.04, 48.97, 35.55, 32.66, 29.16, 28.46, 27.92, 26.90, 26.45, 20.04, 14.16.

ESI-MS: 759.20 (M-1).

Synthesis of 4-((1-(10-azidodecyl)-5-carboxy-3,3-dimethyl-3*H*-indol-1-ium-2-yl)methylene)-2-((-1-butyl-5-carboxy-3,3-dimethylindolin-2-ylidene)methyl)-3-oxocyclobut-1-en-1-olate (5)

4-((1-(10-Bromodecyl)-5-carboxy-3,3-dimethyl-3*H*-indol-1-ium-2-yl) methylene)-2-((-1-butyl-5-carboxy-3,3-dimethylindolin-2-ylidene) methyl)-3-oxocyclobut-1-en-1-olate (0.025 g, 0.033 mmol) and sodium azide (0.0024 g, 0.036 mmol) were added in a vial and dissolved in DMF (1 ml). The vial was sealed and the reaction was carried out in microwave (T = 100 °C, 20 minutes). The product was transferred to a separating funnel with CH_2CI_2 and it was washed with brine and twice with deionized water. Then the product was dried with sodium sulphate and filtered and the solvent was evaporated under vacuum.

Yield: 63% (0.016 g, 0.021 mmol).

^{1}H NMR (200 MHz, DMSO-d6) δ (ppm) = 8.03 (s, 2H), 7.96 (d, 2H, J = 8.0 Hz), 7.43 (d, 2H, J = 8.0 Hz), 5.90 (s, 2H), 4.12 (t,

Table 1 Composition in weight of the formulations and molecules used

	Formulations		
	YNE	EQ	TH
Thiol monomer (wt%) 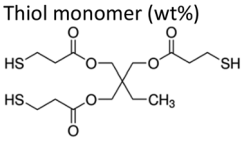	70	77	84
Alkyne monomer (wt%) 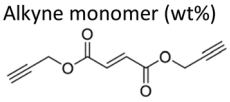	30	23	16
Photoinitiator (wt%) 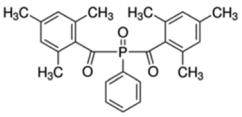	1	1	1

4H, J = 6.0 Hz), 3.47 (t, 2H, J = 7.0 Hz), 1.70 (m, 12H), 1.23 (m, 20H), 0.94 (t, 3H, J = 8.0 Hz).

The compound solubility in $CDCl_3$ proved too low to record a ^{13}C NMR spectrum.

HR-ESI-MS: calculated 720.3839, found 720.3763 (M-1).

Preparation of the printable formulations. Three different formulations were prepared by mixing the synthesized alkyne with the trifunctional thiol chosen. Different ratios of the two components were mixed in order to obtain a stoichiometric formulation (named EQ), one formulation with an excess of triple (named YNE) bonds and the other with an excess of SH groups (named TH, see Table 1). In all the formulations 1 phr (per hundred resin) of BAPO was added and solubilized with the addition of few drops of acetone.

Printing process. A 3DLPrinter-HD 2.0 (Robot Factory) equipped with a projector with a resolution of 50 μm in x and y (1920 × 480 × 1080 pixels) was used as printing apparatus. The Z resolution can be varied from 10 to 100 μm. The power density of the light source is 10 mW cm^{-2}. The irradiation time was set for each formulation according to their reactivity (see ESI†). After printing, a post-curing process (3 min) was performed in air with a broad-band medium pressure mercury lamp, also provided by Robot Factory (UV power density 50 mW cm^{-2}).

Post functionalization process – alkyne fluorescent labelling

An azide terminated squaraine dye was synthesized, able to perform a 'click' chemistry reaction with the alkyne groups available on the 3D printed structure. The idea is to have a sensitive and robust method for observing alkyne free groups exposed in the three different formulations (YNE, EQ and SH) after the 3D printing process. The post functionalization process reaction was performed following the procedure developed by A. B. Hughes *et al.* based on Cu-catalysis in combination with terminal-alkynes.[46] In brief, the sample was added to a solution of 1 mmol azide terminated squaraine dye and Cu(0) powder in a 1 : 2 mixture of *t*BuOH : H_2O. After 2 hours, the 3D printed object was thoroughly washed in ethanol (3 × 5 ml) and dried in a nitrogen stream.

Characterization

Photorheology tests were performed with an Anton Paar rheometer (Physica MCR 302) in parallel plates. The instrument is coupled with a Hamamatsu LC8 lamp emitting in the visible range with a cut-off filter below 400 nm (intensity 10 mW cm^{-2}) and it is equipped with a glass bottom plate and an upper one in aluminium (∅ 25 mm). The formulations containing the mixture of monomers and the photoinitiator were placed on the glass plate, the gap between the two plates was then set to 0.3 mm and the sample was kept at 25 °C, under a constant shear frequency of 10 rad s^{-1} and strain amplitude of 5%. During the test the sample is illuminated from below the glass plate; light is turned on after 1 min in order to stabilize the system. The value of G' as a function of the irradiation time was measured for all the prepared samples.

ATR spectra were collected with a Nicolet iS50 FT-IR spectrometer (Thermo Scientific) equipped with an attenuated total reflection (ATR) accessory (Smart iTX). The spectra were collected firstly on a drop of the liquid photocurable formulations and then on the 3D printed samples after UV post curing. The conversion of the thiol group (peak at 2570 cm^{-1}) and triple (peak at 2130 cm^{-1}) and double bonds (peak at 1640 cm^{-1}) was evaluated calculating the decrease of the areas of the peaks. The spectra were normalized by the stretch of carbonyl group centred at 1720 cm^{-1}.

The thermal behaviour of the monomer was evaluated by DSC analysis using a METTLER DSC-30 (Greifensee, Switzerland) instrument with a ramp from RT to 150 °C (10 °C min^{-1}).

The thermomechanical properties of the printed materials were evaluated by DMA. 3D printed films were prepared (5 × 20 × 0.3 mm) and tested using a Triton Technology TTDMA. The response of the samples was observed in the temperature range of −40 to 70 °C with a heating rate of 3 °C min^{-1}, at a frequency of 1 Hz and a strain of 20 μm.

Bright-field and fluorescence images were collected using a microscope (model Eclipse Ti2 Nikon) coupled with a Crest X-Light spinning disk confocal microscope and a Lumencor SPECTRA X light engine. All images displayed the same scaling and were collected using a Plan Fluor 10 × 0.3 NA and a Plan Apo 20 × 0.75 NA (Nikon). A scan of large images at high magnification was performed in order to have a whole overview of the sample.

Nuclear magnetic resonance ^1H NMR (200 MHz and 600 MHz) and ^{13}C NMR (151 MHz) experiments were conducted using a Bruker AVANCE 200 (200 MHz) and a Jeol ECZ-R 600 MHz instrument with deuterated chloroform (Sigma-Aldrich, 99.8 atom%) and deuterated DMSO. Chemical shifts were referenced to the solvent proton resonance ($CDCl_3$: 7.26 ppm for ^1H NMR and 77.17 ppm for ^{13}C NMR and DMSO: 2.50 ppm for ^1H NMR and 39.52 ppm for ^{13}C NMR).

XPS (X-ray Photoelectron Spectroscopy) measurements have been performed by means of a PHI Versaprobe 5000 (Physical Electronics – Chanhassen, MN – USA), equipped with a monochromatic Al k-alpha source (1486.6 eV). Both survey and high resolution (HR) spectra have been acquired for each sample. A Shirley background function has been applied before each deconvolution procedure for HR spectral analysis, while Voigt functions have been used to perform each fitting procedure. Chemical shifts have been referred to C 1s (C–C) at 284.5 eV. Data have been analysed with CasaXPS software (Version 2.3.18).

Results and discussion

After the synthesis, the alkyne monomer chosen (bis(propargyl) fumarate) was mixed with a trifunctional thiol, in different ratios, in order to obtain formulations with stoichiometric and off-stoichiometric (OSTY) compositions. Before printing, the reactivity of the liquid mixtures was assessed by photorheology tests (see the ESI†). Following the variation of the elastic modulus upon visible light irradiation, it has been possible to observe the polymerization kinetics of the three formulations: while the stoichiometric one (EQ) and the one with the excess of thiols (TH) presented a good reactivity, similar to other formulations already proposed,[47] the formulation with the excess of triple bonds (YNE) needed longer irradiation times. The delayed gelation time in the YNE formulation can be attributed to the lower amount of trifunctional thiol monomers, which act as cross-linkers, allowing rapid creation of a polymer network. Considering the reactivity of the mixtures, different mechanisms occur: with higher thiol concentrations (TH and EQ formulations) an ideal step-growth reaction should occur (see the ESI† for the thiol–yne and thiol–ene reaction scheme) while in thiol-limited samples (YNE) a chain-growth addition mechanism could also occur, *i.e.* homopolymerization of the alkyne/alkene moieties.[38] Considering the different reaction rates of the two mechanisms, different curing times are necessary.

The evaluation of the curing time by photorheology allowed setting the printing parameters (see Table S1 in the ESI†). Firstly, flat specimens (5 × 20 × 0.3 mm) were produced for each single formulation, and then hybrid samples were also obtained by changing the formulation during the printing process; this allowed obtaining samples presenting different excesses of reactive groups on the different sides. Those specimens were both used for ATR, XPS and DMA measurements. The conversion of the reactive groups was evaluated by ATR analysis comparing the spectra of the liquid formulations with those collected on the printed samples. The values of conversion are reported in Table 2 (see the Characterization section for peak assignment; spectra reported in the ESI†).

The alkyne molecule used also presents a vinyl double bond along its chain; this group can also react with one thiol moiety; thus, the conversion of the double bond has also been taken into consideration. Nevertheless its interpretation is relatively complicated since, during the thiol–yne reaction, after the addition of a first thiyl radical to the triple bond, a vinyl sulphide is also temporary generated and thus a concomitant effect is observed.[38]

Table 2 Conversion of the reactive groups present in the formulation by observing the decrease of the thiol (2570 cm^{-1}), alkyne (2130 cm^{-1}) and alkene (1640 cm^{-1}) peaks in ATR spectra

Sample	–SH conversion (%)	–C≡C– conversion (%)	–C=C– conversion (%)
EQ	60	50	72
YNE	80	37	63
TH	48	98	100

The values reported showed that the EQ specimen does not reach full conversion, and it presents both unreacted thiol and triple bonds. This could be expected, considering that once the two monomers react the mobility of the system considerably decreases, preventing further reactions. As a matter of fact, this formulation becomes 3D printable; however, the presence of both the species in a considerable amount makes this material not exploitable for selective functionalization. Differently, both the OSTY formulations present a more controllable behaviour. As expected, the TH formulation presents a complete reaction of unsaturated bonds, since they could react with the thiols present in their proximity. Similarly, the YNE formulation presents a very high conversion of –SH groups and a high number of remaining triple bonds.

In order to support ATR results, XPS analyses have been performed on the EQ, TH and YNE samples. The presence of C, O and S (together with P due to the presence of the photoinitiator) has been highlighted by survey measurements (not reported). Then, HR spectra have been collected in order to specify the residual chemical bonds, especially for off-stoichiometric formulations. C 1s peaks have been deconvoluted into 6 peaks for the EQ and YNE samples and only 3 peaks for the TH one.

Fig. 1A reports the three C 1s peaks, together with the attribution of each chemical shift. According to the literature,[48,49] the C–C peak (peak I) has been assigned to 284.5 eV, while the –C=C– and the –C≡C– bonds have been located respectively at −0.3 eV and at −0.7 eV from the C–C one. The fourth peak at 1.20 eV from peak I has been assigned to C–O/C–N/C–S bonds, while the fifth one at 2.50 eV to C=O and the sixth and last one at 3.80 eV to C–O–C=O. Table 3 reports the relative % due to –C=C– and –C≡C– chemical shifts, in order to make a comparison with ATR results. It is necessary to point out that since the two techniques have different in-depth sensitivities, the % could not be exactly the same (XPS can sample the first 10 nm maximum from the rear surface, while ATR can sample several microns). Nevertheless, it is possible to find an accordance between the two sets of data, since the sample with the higher % of –C≡C– is YNE, which is the one with the lowest –C≡C– conversion according to ATR measurements. Regarding the –C=C– % the sample with the lowest amount is the TH one, which has shown a 100% complete conversion,

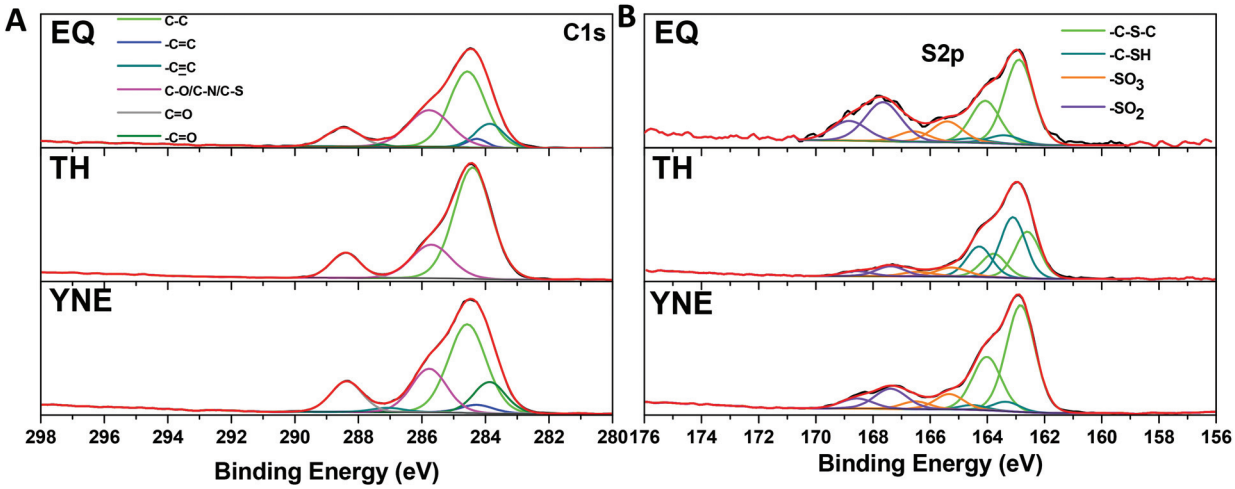

Fig. 1 HR XPS spectra for EQ, TH and YNE samples: (A) C 1s peaks and (B) S 2p doublets with their deconvolution curves.

Table 3 Chemical bonds % evaluated by means of HR XPS spectral deconvolution for S 2p (unbound thiol –SH) and C 1s (–C≡C– and –C=C– chemical shifts) photoelectron peaks

Sample	–SH (%)	–C≡C– (%)	–C=C– (%)
EQ	5.5	11.9	3.0
YNE	5.7	13.8	3.7
TH	46.7	<0.1	<0.1

together with the –C≡C– contribution. In fact, for the sample TH, the two peaks related to these chemical shifts have not been inserted: by maintaining the same FWHM of the C–C peak for all the samples, it is not needed to further add the two contributions related to unsaturated C bonds to get the best fit.

Regarding the thiol groups, the S 2p photoelectron peaks have been checked for each sample. We have used four doublets (S $2p_{3/2}$ and S $2p_{1/2}$, 1.18 eV separated one to each other) in order to perform the best deconvolution procedure. The first doublet, located at 162.8 eV, has been assigned to the bound thiol group, as reported in several papers.[50–52] The second doublet, at 163.3 eV, has been related to the unbound thiol group, which means that the –SH termination is free and available for further reactions. The third doublet at 165.3 eV is due to $-SO_3$, while the last one at 167.4 eV is due to the $-SO_2$ bond. In Table 3 the % due to unbound thiol is reported. The sample with the highest concentration is the TH one, in accordance with ATR results, which show that TH is the sample with the lowest conversion rate.

The results obtained with different techniques for the different reactive moieties are in line with the literature; Faribanks *et al.*[38] measured the evolution of the concentration of the functional groups in OSTY reactions and showed that, after polymerization, when the alkyne is in excess, besides the presence of residual triple bonds, the presence of vinyl groups is higher than in stoichiometrically balanced formulations, while no vinyl groups were observed in the formulation containing the excess of thiol which shows a relatively high amount of SH groups.

The printed flat specimens were also tested by Dynamic Mechanical Analysis, DMA (see Fig. 2); different matrices showed even a different thermal-mechanical behaviour. DMA measurements showed that the 3D printed materials presented a higher glass transition temperature (T_g) by increasing the amount of the yne monomer in the formulation, moving from 8 °C in the TH sample to 34 °C in the YNE one. This could be explained taking into account that the yne monomer gives rigidity to the system (see DSC of the monomer in the ESI†). This effect could be used to tune the desired properties of the final object. Moreover, a bilayer specimen was produced, changing the printable formulation at half of the printing process. As expected, the sample presented the two T_gs of the two off-stoichiometric materials, indicating that it is possible to print

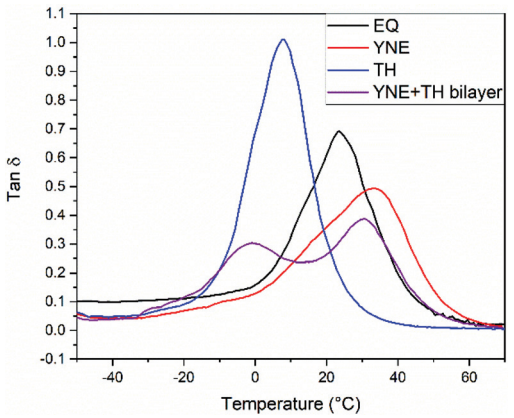

Fig. 2 Tan δ plot obtained by DMA on flat specimens produced with the three formulations (off-stoichiometric TH, off-stoichiometric YNE and stoichiometric EQ) and on one bilayer specimen built with the two OSTY formulations one after the other (TH and YNE).

consecutively the two formulations maintaining their distinct properties.

The studied formulations allowed printing parts of different shapes with a good resolution (smallest features ~300 μm *X*–*Y* plane, see Fig. 3). Furthermore, just by changing the formulation during the printing process, it has been possible to obtain objects exposing different functional groups (–SH or alkyne) along their *z* axis (Fig. 3). No delamination during printing was observed and good adhesion of the different layers was also maintained after the post curing process, which was demonstrated by an easy handling of the hybrid materials.

The residual functional groups, whose presence was evaluated by ATR and XPS analysis, can be exploited for further functionalization steps; in a previous study Hoffmann *et al.*[43] exploited unreacted thiol moieties from a 3D printed OSTE formulation to graft propargyl acrylate on a printed surface and subsequently exploited the triple bond to link a fluorescent dye containing azide. In this work, as a proof of concept, the alkyne groups still available on the printed parts have directly been exploited in the functionalization step with the synthesized azide terminated squaraine dye.

Thus, by choosing a dye, which selectively reacts towards the alkyne groups still available in the 3D printed object, we demonstrated that the printed structures can be easily and specifically functionalized. As expected from previously described analysis and conversion of the reactive groups, the triple bonds were available in different amounts in the three formulations according to their composition (TH, EQ and YNE).

In Fig. 3A, the results of the post functionalization step with the azide terminated squaraine dye for the 3D printed object obtained starting from the three selected printable formulations, two off-stoichiometric formulations (YNE and TH) and one stoichiometric formulation (EQ). As stated, a trend in the colour change, from native white to blue (due to the presence of squaraine dye), of the three different specimens was evident. In particular, there was no evidence of dye functionalization in the off-stoichiometric TH sample, while there was an increasing dye linkage in the EQ and OSTY YNE, respectively.

To further demonstrate the selectivity of the post functionalization, due to the azide terminated squaraine dye reacting with the OSTY YNE, a fluorescent imaging study was performed on a slice obtained from the hybrid structure (Fig. 3D). The sample was selected along the *z* axis (hybrid structure with the two OSTY formulations), in order to be representative of the whole 3D printed object. When the fluorescence dye (azide terminated squaraine) was grafted on the specimen, it was possible to produce a fluorescence image of the different printed layers.

To provide a wider field-of-view, a large image was produced (72 scans with a 10× objective), as shown in Fig. 4. The wide field fluorescence image (Fig. 4B) clearly shows the different triple bond conversion, between the two OSTY formulations. The blue fluorescence signal due to squaraine dye functionalization was really intense in the YNE part (top of the image) and only barely visible in the TH area (bottom of the image). As a result, the fluorescence study exhibits a sharp edge in the interface area, verifying the possibility of selectively functionalizing the 3D printed object, only by changing along the *z*-axis the stoichiometry of the formulations.

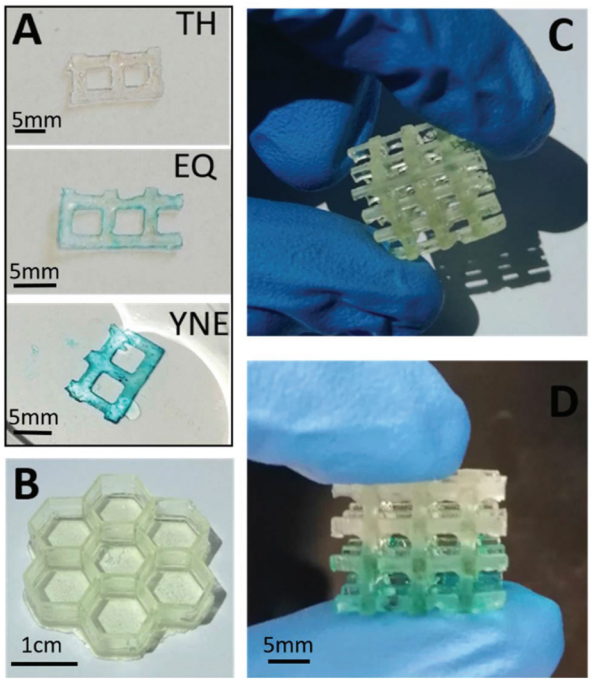

Fig. 3 Images of the 3D printed objects. (A) Result of the post functionalization step with the squaraine dye for the three formulations (off-stoichiometric TH, off-stoichiometric YNE and stoichiometric EQ). (B) Structure built with the stoichiometric formulation (EQ), (C) hybrid structure with the two off stoichiometric formulations (YNE at the bottom and TH at the top), and (D) result of the post functionalization process on the same structure.

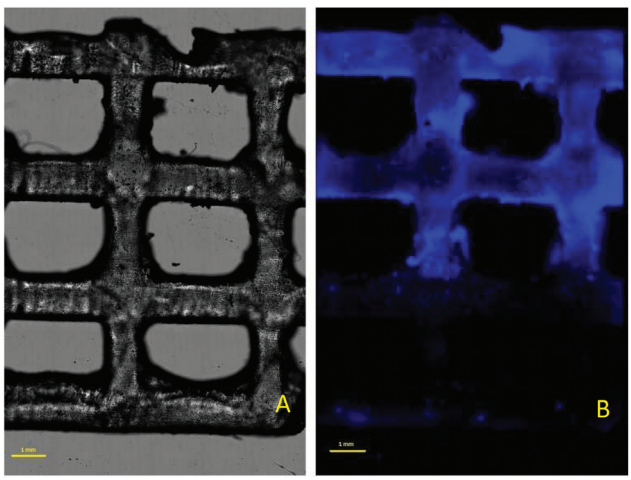

Fig. 4 Wide field optical detection (A – bright field and B – fluorescence) of the slice obtained from the 3D printed hybrid structure (scale bar 1 mm). The sample was functionalized with a solution of 1 mmol of azide terminated squaraine.

Conclusions

In this work, we demonstrated that thiol–yne chemistry is an available strategy for the production of new 3D printable materials. Moreover, the development of off-stoichiometric thiol–yne formulations (OSTY) allows the possibility of locally tuning the characteristics of the network, exposing selectively desired moieties (either alkyne or thiol groups) that could be exploited for a further functionalization step. We reached this goal by successful grafting of squaraine dyes with azide moieties.

The strategy proposed here opens a new perspective for the fabrication of functional 3D printed structures, in particular for the biomedical field in which multiple functionalizations could be a key-point to the development of next generation devices.

Conflicts of interest

There are no conflicts to declare.

Acknowledgements

The present work was performed in the framework and financed by POLITO BIOMed LAB, an interdepartmental laboratory financed by Politecnico di Torino, DEFLeCT ("Advanced platform for the early detection of not small cells lung cancer", Piedmont "Health & WellBeing" Platform) project, funded by Regione Piemonte POR-FESR 2014–2020, and HYDROLIGHT ("Reversible 3D light-structuring of stimuli-responsive hydrogel networks for biophotonic applications"), funded by Politecnico di Torino 2017–2019.

We warmly acknowledge Prof. Silvia Bordiga for the fruitful discussions we had with her on the topic.

Notes and references

1 T. D. Ngo, A. Kashani, G. Imbalzano, K. T. Q. Nguyen and D. Hui, *Composites, Part B*, 2018, **143**, 172–196.
2 B. C. Gross, J. L. Erkal, S. Y. Lockwood, C. Chen and D. M. Spence, *Anal. Chem.*, 2014, **86**, 3240–3253.
3 R. L. Truby and J. A. Lewis, *Nature*, 2016, **540**, 371.
4 S. C. Ligon, R. Liska, J. Stampfl, M. Gurr and R. Mülhaupt, *Chem. Rev.*, 2017, **117**, 10212–10290.
5 M. Hofmann, *ACS Macro Lett.*, 2014, **3**, 382–386.
6 N. Bhattacharjee, A. Urrios, S. Kang and A. Folch, *Lab Chip*, 2016, **16**, 1720–1742.
7 E. Cuan-Urquizo, E. Barocio, V. Tejada-Ortigoza, B. R. Pipes, A. C. Rodriguez and A. Roman-Flores, *Materials*, 2019, **12**, 895.
8 F. Shen, S. Yuan, C. K. Chua and K. Zhou, *J. Mater. Process. Technol.*, 2018, **254**, 52–59.
9 A. Bagheri and J. Jin, *ACS Appl. Polym. Mater.*, 2019, **1**, 593–611.
10 J. Zhang and P. Xiao, *Polym. Chem.*, 2018, **9**, 1530–1540.
11 A. Bandyopadhyay and S. Bose, *Additive Manufacturing*, CRC Press, 2015.
12 J.-Y. Lee, J. An and C. K. Chua, *Appl. Mater. Today*, 2017, **7**, 120–133.
13 M. Nadgorny and A. Ameli, *ACS Appl. Mater. Interfaces*, 2018, **10**, 17489–17507.
14 Z. X. Khoo, J. E. M. Teoh, Y. Liu, C. K. Chua, S. Yang, J. An, K. F. Leong and W. Y. Yeong, *Virtual Phys. Prototyp.*, 2015, **10**, 103–122.
15 M. Layani, X. Wang and S. Magdassi, *Adv. Mater.*, 2018, **30**, 1706344.
16 G. Gonzalez, A. Chiappone, I. Roppolo, E. Fantino, V. Bertana, F. Perrucci, L. Scaltrito, F. Pirri and M. Sangermano, *Polymer*, 2017, **109**, 246–253.
17 V. C.-F. Li, X. Kuang, A. Mulyadi, C. M. Hamel, Y. Deng and H. J. Qi, *Cellulose*, 2019, **26**, 3973–3985.
18 J. Bustillos, D. Montero-Zambrano, A. Loganathan, B. Boesl and A. Agarwal, *Polym. Compos.*, 2019, **40**, 379–388.
19 R. T. Shafranek, S. C. Millik, P. T. Smith, C.-U. Lee, A. J. Boydston and A. Nelson, *Prog. Polym. Sci.*, 2019, **93**, 36–67.
20 G. Scordo, V. Bertana, L. Scaltrito, S. Ferrero, M. Cocuzza, S. L. Marasso, S. Romano, R. Sesana, F. Catania and C. F. Pirri, *Mater. Today Commun.*, 2019, **19**, 12–17.
21 M. Zarek, M. Layani, I. Cooperstein, E. Sachyani, D. Cohn and S. Magdassi, *Adv. Mater.*, 2016, **28**, 4449–4454.
22 F. Frascella, G. González, P. Bosch, A. Angelini, A. Chiappone, M. Sangermano, C. F. Pirri and I. Roppolo, *ACS Appl. Mater. Interfaces*, 2018, **10**, 39319–39326.
23 I. Roppolo, A. Chiappone, A. Angelini, S. Stassi, F. Frascella, C. F. Pirri, C. Ricciardi and E. Descrovi, *Mater. Horiz.*, 2017, **4**, 396–401.
24 H. H. Hwang, W. Zhu, G. Victorine, N. Lawrence and S. Chen, *Small Methods*, 2018, **2**, 1700277.
25 F. Abbasi, H. Mirzadeh and A.-A. Katbab, *Polym. Int.*, 2001, **50**, 1279–1287.
26 S. Stassi, E. Fantino, R. Calmo, A. Chiappone, M. Gillono, D. Scaiola, C. F. Pirri, C. Ricciardi, A. Chiadò and I. Roppolo, *ACS Appl. Mater. Interfaces*, 2017, **9**, 19193–19201.
27 X. Wang, X. Cai, Q. Guo, T. Zhang, B. Kobe and J. Yang, *Chem. Commun.*, 2013, **49**, 10064–10066.
28 J. M. Goddard and J. H. Hotchkiss, *Prog. Polym. Sci.*, 2007, **32**, 698–725.
29 R. M. Arnold, N. E. Huddleston and J. Locklin, *J. Mater. Chem.*, 2012, **22**, 19357–19365.
30 R. M. Hensarling, V. A. Doughty, J. W. Chan and D. L. Patton, *J. Am. Chem. Soc.*, 2009, **131**, 14673–14675.
31 H. Nandivada, X. Jiang and J. Lahann, *Adv. Mater.*, 2007, **19**, 2197–2208.
32 A. B. Lowe, C. E. Hoyle and C. N. Bowman, *J. Mater. Chem.*, 2010, **20**, 4745–4750.
33 K. Griesbaum, *Angew. Chem., Int. Ed. Engl.*, 1970, **9**, 273–287.
34 A. B. Lowe, *Polymer*, 2014, **55**, 5517–5549.

35 A. Massi and D. Nanni, *Org. Biomol. Chem.*, 2012, **10**, 3791–3807.
36 J. W. Chan, J. Shin, C. E. Hoyle, C. N. Bowman and A. B. Lowe, *Macromolecules*, 2010, **43**, 4937–4942.
37 C. E. Hoyle and C. N. Bowman, *Angew. Chem., Int. Ed.*, 2010, **49**, 1540–1573.
38 B. D. Fairbanks, T. F. Scott, C. J. Kloxin, K. S. Anseth and C. N. Bowman, *Macromolecules*, 2009, **42**, 211–217.
39 A. Oesterreicher, C. Gorsche, S. Ayalur-Karunakaran, A. Moser, M. Edler, G. Pinter, S. Schlögl, R. Liska and T. Griesser, *Macromol. Rapid Commun.*, 2016, **37**, 1701–1706.
40 A. Oesterreicher, J. Wiener, M. Roth, A. Moser, R. Gmeiner, M. Edler, G. Pinter and T. Griesser, *Polym. Chem.*, 2016, **7**, 5169–5180.
41 C. F. Carlborg, T. Haraldsson, K. Öberg, M. Malkoch and W. van der Wijngaart, *Lab Chip*, 2011, **11**, 3136–3147.
42 F. Saharil, C. F. Carlborg, T. Haraldsson and W. van der Wijngaart, *Lab Chip*, 2012, **12**, 3032–3035.
43 A. Hoffmann, H. Leonards, N. Tobies, L. Pongratz, K. Kreuels, F. Kreimendahl, C. Apel, M. Wehner and N. Nottrodt, *J. Tissue Eng.*, 2017, **8**, 1–9.
44 E. R. Gillies, B. Fan, A. D. WongJohn and F. Trant, US10214609B2, 2019.
45 N. Barbero, C. Magistris, J. Park, D. Saccone, P. Quagliotto, R. Buscaino, C. Medana, C. Barolo and G. Viscardi, *Org. Lett.*, 2015, **17**, 3306–3309.
46 O. D. Montagnat, G. Lessene and A. B. Hughes, *Tetrahedron Lett.*, 2006, **47**, 6971–6974.
47 A. Chiappone, I. Roppolo, E. Naretto, E. Fantino, F. Calignano, M. Sangermano and F. Pirri, *Composites, Part B*, 2017, **124**, 9–15.
48 D. Briggs and G. Beamson, *Anal. Chem.*, 1992, **64**, 1729–1736.
49 N. S. Bhairamadgi, S. Gangarapu, M. A. Caipa Campos, J. M. J. Paulusse, C. J. M. van Rijn and H. Zuilhof, *Langmuir*, 2013, **29**, 4535–4542.
50 D. G. Castner, K. Hinds and D. W. Grainger, *Langmuir*, 1996, **12**, 5083–5086.
51 J. Jia, A. Kara, L. Pasquali, A. Bendounan, F. Sirotti and V. A. Esaulov, *J. Chem. Phys.*, 2015, **143**, 104702.
52 L. Pasquali, F. Terzi, R. Seeber, S. Nannarone, D. Datta, C. Dablemont, H. Hamoudi, M. Canepa and V. A. Esaulov, *Langmuir*, 2011, **27**, 4713–4720.